Interplay between geometrical structure and electronic properties in rippled free-standing graphene

P. Partovi-Azar,[1] N. Nafari,[2,3] and M. Reza Rahimi Tabar[3,4]

[1]*Computational Physical Science Laboratory, Department of Nano-Science, Institute for Research in Fundamental Sciences (IPM), P.O. Box 19395-5531, Tehran, Iran*

[2]*School of Physics, Institute for Research in Fundamental Sciences (IPM), P.O. Box 19395-5531, Tehran, Iran*

[3]*Department of Physics, Sharif University of Technology, 11365-9161, Tehran, Iran*

[4]*Fachbereich Physik,Universität Osnabrück, Barbarastraße 7, 49076 Osnabrück, Germany*

(Received 6 March 2011; published 22 April 2011)

It has been argued that the electron-hole puddles formed on graphene are mostly due to substrate-induced charged impurities [J. Martin *et al.*, Nature Phys. **4**, 144 (2008),Y. Zhang *et al.*, Nature Phys. **5**, 722 (2009)]. Here, using first-principles *ab initio* calculations, we show that the existence of ripples and electron-hole puddles is indeed an intrinsic property of graphene at finite temperatures. We found a relatively large correlation between the electronic charge density distribution on the surface of graphene and its local geometrical properties, such as local mean curvature and average bond length. We show that the electron and hole puddles appear in places where curvatures are large and small, respectively. We also determined the average sizes of the observed electron-hole puddles and have reported their percolating nature.

DOI: 10.1103/PhysRevB.83.165434 PACS number(s): 61.48.Gh, 71.15.Pd, 82.45.Mp, 73.22.Pr

I. INTRODUCTION

Graphene, a transparent single layer of carbon atoms arranged in a hexagonal, honeycomb structure,[1] has attracted the attention of a great number of researchers. In fact, owing to graphene's unique properties, such as its linear energy dispersion relation and its two-dimensional lattice structure, various interesting phenomena have been experimentally observed and theoretically studied. Among the salient effects and characteristics of graphene, one may mention the quantum Hall effect,[2] ultrahigh mobility,[3] superior thermal conductivity,[4] high mechanical strength,[5] observation of plasmarons,[6] and electron-hole puddles.[7] These unusual properties have lead many researchers working in this field to forecast a promising future use of graphene as the building block of nanoelectronic devices (for more recent works see Refs. 8–12).

Recently, electron-hole puddles have been observed for graphene on a Si/SiO_2 wafer.[7] The observed transport properties of graphene sheets at zero magnetic field can be explained by scattering from electron-hole puddles[13] (see also Refs. 14 and 15). It has been recently argued that the chemical potential variations on graphene are *probably* due to charged impurities above and below the layer, substrate-induced structural distortions, and chemical doping from residing residues.[16] Moreover, some authors, using modified Hamiltonians for Kohn-Sham-Dirac density functional theory,[17] or focusing on the membrane properties of graphene,[18] have provided several pictures regarding the connection between the charge density distribution on graphene and its structural properties. However, the authors in Ref. 17 did not observe an evident correlation between the spatial distribution of the electron-hole puddles and the out-of-plane topographic corrugations. As far as we know, the rippled structure of graphene has been obtained by using the Monte Carlo method and/or molecular dynamics (MD) simulations employing a parametric interatomic potential, or by modeling the rippled structure in the form of a mathematical function, such as a sinusoidal wave or a Gaussian function.[17–21] In this paper, without calling upon any modifications to the quasiparticle Kohn-Sham Hamiltonian[22] or upon the use of any parametric interatomic potentials, we have employed an *ab initio* first-principles scheme based on density functional theory (DFT) to study the formation of the ripples as well as the electronic features induced by them. We started from a flat free-standing graphene sheet with 450 carbon atoms, namely, a sheet without external stresses and free from interactions with substrate or impurities, and performed an *ab initio* MD simulation. After we obtained the rippled structure, we then performed the electronic structure calculation. We found a relatively strong correlation between the electronic charge density of the states near the Fermi level and the local curvature of the surface. Furthermore, the charge density related to the more energetic electronic states, far from the Fermi level, has been shown to anticorrelate mostly with the average bond length. Moreover, the induced electron-hole puddles, their average area, and their percolating nature are also discussed.

This paper is organized as follows: In Sec. II, we outline the computational method that we use. Results are presented in Sec. III and the related discussions follow afterward. Finally, we summarize our results and present our conclusions in Sec. IV.

II. METHOD OF CALCULATION

Through our first-principles *ab initio* calculations, we first performed an *ab initio* mixed-forces molecular dynamics simulation[23,24] at finite temperature, $T = 300$ K, by means of Nosé-Hoover thermostat.[25] The time step length, Δt, for the MD simulation was 0.1 fs. In general, this value should be less than the time scale related to the highest vibrational frequency of the system (the reported value for the highest vibrational frequency for graphene is between $\approx$1570 and $\approx$1700 cm^{-1} at the Γ point[26]). The simulation ran for 2×10^5 time steps giving a total MD time of 20 ps. We have benefited from the order-N method implemented in the SIESTA density functional code,[27] which allowed our computations to be performed efficiently. We used a Troullier-Martins type pseudopotential[28] for carbon

with a double-ζ, singly polarized orbital for the basis set along with a $6 \times 6 \times 1$ Monkhorst-Pack grid[29] in the reciprocal lattice. In the MD simulation, only the Γ point was used for the Brillouin zone integration, which was found to give a nearly converged geometry for graphene when compared with calculations using large k-point integration meshes for smaller samples. We also employed periodic boundary conditions. It is well known that the local density approximation (LDA) for the exchange-correlation energy functional E_{XC} works well for nearly homogeneous electronic systems, whereas the generalized gradient approximation (GGA) for the E_{XC} should work better than the LDA for systems with considerable electronic density variations. Therefore, for the purpose of studying the charge inhomogeneity on the surface of graphene in the form of electron-hole puddles, it is appropriate to use the GGA. We have also used Perdew-Burke-Ernzerhof parametrization, which usually gives good results for carbon-based structures in comparison with experimental data.[30] The *ab initio* MD phase was used for two systems. The first one consisted of 1250 atoms. In this case, the electronic structure calculations were not carried out. The second sample consisted of 450 atoms for which the electronic structure calculations were performed.[31] In order to find the correlations between the structural features and the charge density, we first employed a thermal averaging by using the *kernel* method to smooth the height fluctuations. According to the kernel method, one considers a kernel function $K(u,v)$ that satisfies the condition $\int_{-\infty}^{+\infty} du \int_{-\infty}^{+\infty} dv K(u,v) = 1$, such that the data [here, the z component of the coordinates of the atoms: $z \equiv z(x,y)$] are smoothed by

$$z(x,y) = \frac{1}{nh} \sum_{i=1}^{n} z(x_i,y_i) K\left(\frac{x-x_i}{h}, \frac{y-y_i}{h}\right), \qquad (1)$$

where h is the window width and n runs through the neighbors including the atom under consideration. One of the most useful kernels is $K(u,v) = (2\pi)^{-1} \exp[-\frac{1}{2}(u^2+v^2)]$.[32] Here, we have chosen $h \simeq 3$ Å. Moreover, by considering the projected density of states (PDOS) of π and σ orbitals, we have been able to calculate the π and σ charge densities (CDs) using

$$\rho^i = \sum_m \int_{-\infty}^{E_F} g^{(i,m)}(\epsilon) f(\epsilon)\, d\epsilon, \qquad (2)$$

where $f(\epsilon)$ is the Fermi-Dirac distribution function, $g^{(i,m)}(\epsilon)$ is the projected density of states for the mth orbital of the ith atom at energy ϵ, defined by

$$g^{(i,m)}(\epsilon) = \sum_n \delta(\epsilon - \epsilon_n) \left| \langle \phi_m^i | \Psi_n \rangle \right|^2, \qquad (3)$$

and the Ψ_n's are the Kohn-Sham orbitals. Afterward, the smoothing of these densities was carried out by the same kernel method. In order to obtain the local curvature of the surface, we calculated the Laplacian of the surface, $z \equiv z(x,y)$, taking the second nearest neighbors into account. Starting from

$$z(\vec{r} + \vec{a}') = \sum_{n=0}^{\infty} \frac{(\vec{a}' \cdot \vec{\nabla})^n z(\vec{r})}{n!} \qquad (4)$$

and expanding the summation up to the second nearest neighbors[33] for the graphene honeycomb lattice, we are led to the following relation:

$$\nabla^2 z(x_0,y_0) = \frac{2}{3a'^2} \left(\sum_{i=1}^{6} z(x_i,y_i) - 6z(x_0,y_0) \right), \qquad (5)$$

where $\vec{a}'$ goes from the atom under consideration to the six second nearest neighbors.

III. RESULTS AND DISCUSSION

As shown in Fig. 1(a), our graphene sample, consisting of 1250 carbon atom, obtains a rippled structure during the MD phase with average wavelength of $\lambda \simeq 55$ Å (Ref. 34) and amplitude of $\simeq 0.4$ nm at temperature $T = 300$ K, results which are in agreement with Refs. 19 and 20. The time scale of the shape variation of the ripples is much longer than that of the thermal fluctuations of the individual atoms.

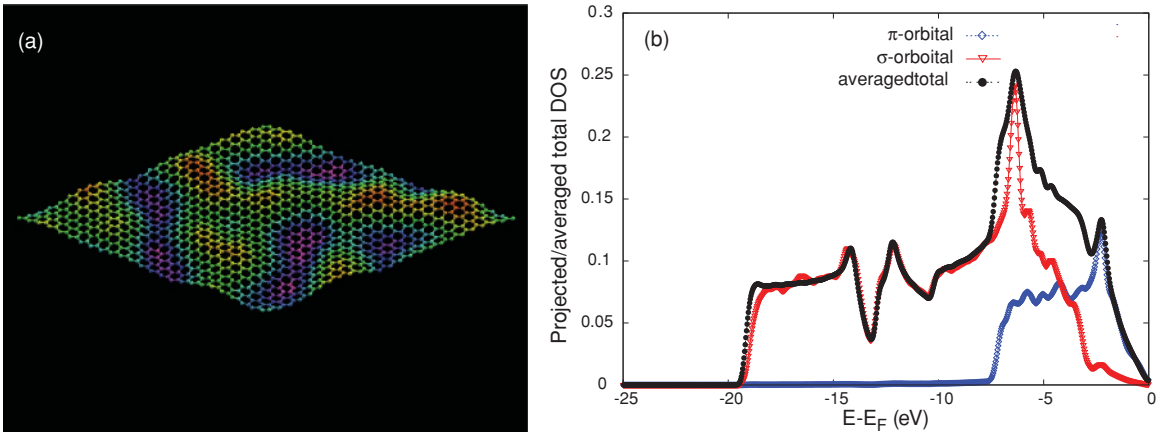

FIG. 1. (Color online) (a) Configuration of a graphene sheet consisting of 1250 carbon atoms at 300 K, obtained by *ab initio* molecular dynamics simulation, without carrying out the electronic structure calculation. Colors indicate the height of the atoms. (b) Projected and averaged total density of states for one of the atoms in a graphene sheet consisting of 450 carbon atoms. Blue diamonds (red triangles) correspond to π orbitals (σ orbitals). Total density of states divided by the number of atoms is shown with black circles. The presented results suggest that the contribution of the σ orbitals to the total charge density is much more than that of the π orbitals.

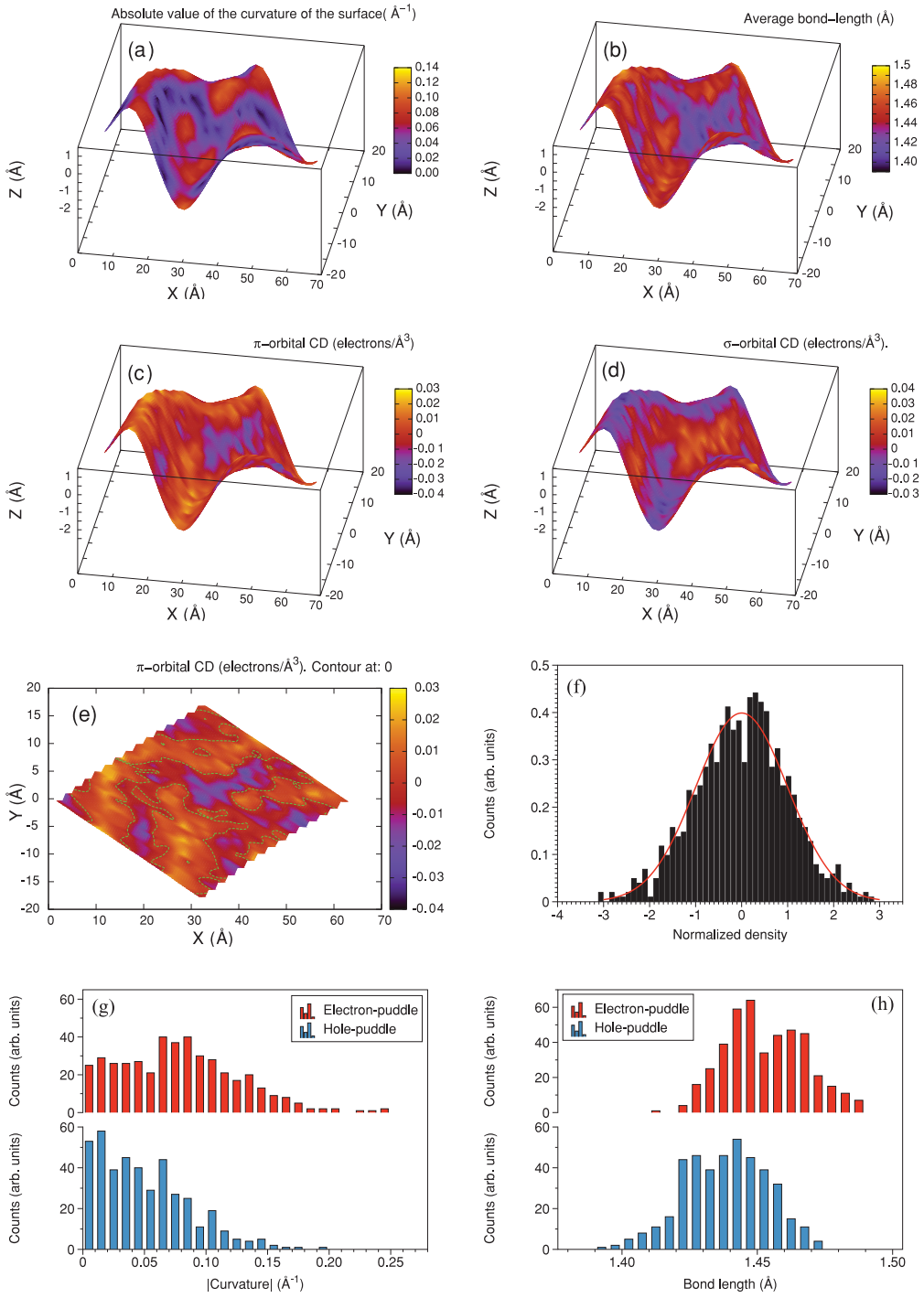

FIG. 2. (Color online) (a) Twice the absolute value of the mean curvature of the graphene surface, i.e., $|\nabla^2 Z(x,y)|$, and (b) the average bond length. (c) and (d) The π and the σ orbital charge density distributions subtracted from their average value in each case, respectively. (e) Color map of the spatial density variations of the π orbital charge density. The green dashed lines show the zero-density contours separating the electron puddles from their adjacent hole puddles. (f) The histogram of the normalized π orbital charge density, i.e., the charge density divided by its variance, and the red line is a Gaussian function with variance equal to 1, which is shown for comparison purposes. (g) shows the distributions of the absolute value of the mean curvature for the hole and the electron puddles. (h) The bond length distribution for the electron and the hole puddles.

Also, there is small-scale roughness appearing on the ripples, due to thermal fluctuations. The amplitude of such height fluctuations, as expected, is very small relative to the ripple sizes.[20]

Figure 1(b) shows the PDOSs for π and σ orbitals of one of the carbon atoms in a graphene sheet consisting of 450 carbon atom, with blue diamonds and red triangles, respectively. The total density of states divided by the number of atoms is

also shown by black circles. In fact, what a nanoprobe, e.g., scanning tunneling microscope (STM), scans is mainly the local density of states of the π band near the Fermi level. However, on atomic scales, i.e., on length scales of the order of C-C bond lengths ($\approx$1.4 Å), what affects the CD lying along a C-C bond is mainly the change in the bond length, affecting the overlap between σ orbitals, rather than the curvature of the surface, which changes the overlap between the π orbitals. This feature hardly shows up in the STM studies.[16] So, in order to simulate the scanning single-electron transistor or STM results which have been mainly reported in experimental studies of the CD distribution on corrugated samples,[7,16] here we separate the contributions of π and σ orbitals to the CD, and study the π contribution mainly.

Figures 2(a) and 2(b) show the absolute value of the mean curvature and the average C-C bond length at each point on the smoothed surface. The curvature and bond lengths are plotted after applying one level of kernel smoothing on the z components of the atoms. Figures 2(c) and 2(d) show the π and σ orbital CDs, respectively. The CD values are subtracted from the corresponding average charge densities, and the electron- and hole-rich regions (puddles) are shown in different colors. The CDs are given in units of electrons/Å^3.

The correlation between the π orbital CDs and the absolute value of the mean curvature (AVMC) is about 67%. The anticorrelation between the σ orbital CDs and the average bond length is $\approx$71%, confirming the fact that the σ orbital CD decreases as the bond length increases.

Figure 2(e) shows the map view of the π orbital CD and the green dashed lines are the contours of the zero CD. The contours highlight the border between adjacent electron and hole puddles. We note that the electron and hole puddles on free-standing graphene have a percolating nature, similar to the experimental observation for a graphene sample on a Si wafer.[7] Figure 2(f) shows the histogram of the normalized π orbital CD, i.e., the charge density divided by its variance. The red curve in Fig. 2(f) is a Gaussian function with variance equal to 1 which is shown for comparison purposes. The histogram shows an asymmetry similar to the experimental results.[7] The skewness of the π orbital CD is about -0.08, which indicates to what extent the probability distribution function of the π orbital CD is an asymmetric distribution. The negative sign of the skewness shows higher probabilities for higher hole densities. The variance of the π orbital CD is about 0.0084 electrons/Å^3. Its average and the variance for electron puddles are 0.0063 and 0.0047 electrons/Å^3, respectively. For hole puddles we find the mean and variance of the π orbital CD to be -0.0074 and 0.0050 electrons/Å^3, respectively.

As mentioned before, by considering the mean values of π orbital CDs for electron-hole puddles as well as total charge neutrality, we conclude that the average size of the hole puddles is smaller than that of the electron puddles. Using a triangulation technique, we find the ratio of $\langle A_{\text{hole}}\rangle$ / $\langle A_{\text{electron}}\rangle \simeq 0.85$, where $\langle A_{\text{electron/hole}}\rangle$ is the mean area of electron and hole puddles. We note that the longer bond lengths in electron puddles result in smaller total overlap of π and σ orbitals at each site. This is confirmed by our computations yielding smaller kinetic energy per particle in this region, and giving rise to larger average distance between the electrons. Finally, this in turn yields lower electron density, and as a consequence, results in a larger area occupied by electron puddles. A similar argument holds for the hole puddles.

Figure 2(g) is a plot of the distributions of the AVMC for the electron and the hole puddles. We find that the average AVMC in the electron puddle is about 0.08/Å and the average AVMC in the hole puddle is about 0.050/Å. The AVMC in the electron puddle is nearly twice as large as the AVMC in the hole puddle. Figure 2(h) shows the bond length distribution for the electron and hole puddles. The total average bond length is $\simeq$1.438 Å. For electron and hole puddles we find the mean bond length to be 1.447 and 1.426 Å, respectively. Therefore, as shown in these figures, we conclude that the hole puddles on the free-standing graphene take form in the regions with shorter bond lengths and smaller curvatures, and electron puddles occur in the regions with longer bond lengths and larger curvatures. As we argued earlier, the hopping energies in the hole puddles are, on the average, larger than the ones in the electron puddles. This results in slightly wider hole bands and slightly narrower electron bands.

IV. CONCLUSIONS

In summary, here, we have tried to approach the problem of the formation of the ripples and the induced charge inhomogeneity on a free-standing graphene sheet in a more fundamental way, by using a DFT-level molecular dynamics simulation and calculating the electronic structure of the system. We observed that, at finite temperatures, the local stress caused by the thermal fluctuations of the atoms will guarantee the formation of ripples on the surface. The time scale of the shape variation of the ripples has been observed to be much longer than that of the thermal fluctuations of the individual atoms. The nonuniform distributions of the local curvature and the bond length, caused by the ripples, have been shown to be the sources of the formation of the electron-hole puddles on the free-standing graphene sheet. In other words, *the formation of the electron-hole puddles is to an intrinsic property of graphene*. These electron-hole puddles have a percolating nature. Furthermore, the kinetic energy of the holes in the hole puddles has been observed to be greater than that of the electrons in the electron puddles. The results show that by using the topographic information of graphene sheets (which could be measured relatively more easily than the local electronic structure) one could more or less locate the positions of the electron-hole puddles and hence the local electronic structure.

ACKNOWLEDGMENTS

We thank A. K. Geim, A. H. MacDonald, P. Maaß, and R. Asgari for very important comments on this work and fruitful discussions. We also would like to thank M. Farjam, A. Namiranian, N. Abedpour, A. Qaiumzadeh, T. Jadidi, and A. Rastkar for useful discussions. Moreover, we thank the Molecular Simulation Laboratory of AUTM, and the Computational Nanotechnology Supercomputing center at IPM for providing the high-performance computation facilities. This work was partially supported by the DFG through Grant No. 190/135-1.

[1] K. S. Novoselov, D. Jiang, F. Schedin, T. J. Booth, V. V. Khotkevich, S. V. Morozov, and A. K. Geim, Proc. Natl. Acad. Sci. USA **102**, 10451 (2005); K. S. Novoselov, A. K. Geim, S. V. Morozov, D. Jiang, M. I. Katsnelson, I. V. Grigorieva, S. V. Dubonos, and A. A. Firsov, Nature (London) **438**, 197 (2005); A. K. Geim and K. S. Novoselov, Nature Mater. **6**, 183 (2007); M. I. Katsnelson and A. K. Geim, Philos. Trans. R. Soc. Ser. A **366**, 195 (2008); Andrey K. Geim and Allan H. MacDonald, Phys. Today **60**(8), 35 (2007); A. H. Castro Neto, F. Guinea, N. M. R. Peres, K. S. Novoselov, and A. K. Geim, Rev. Mod. Phys. **81**, 109 (2009).

[2] K. S. Novoselov, Z. Jiang, Y. Zhang, S. V. Morozov, H. L. Stormer, U. Zeitler, J. C. Maan, G. S. Boebinger, P. Kim, and A. K. Geim, Science **315**, 1379 (2007); Y. Zhang, Y. W. Tan, H. L. Stormer, and P. Kim, Nature (Lonodn) **438**, 201 (2005).

[3] X. Du, I. Skachko, A. Barker, and E. Y. Andrei, Nature Nanotechnol. **3**, 491 (2008).

[4] A. A. Balandin, S. Ghosh, W. Bao, I. Calizo, D. Teweldebrhan, F. Miao, and C. N. Lau, Nano Lett. **8**, 902 (2008); J. H. Seol, I. Jo, A. L. Moore, L. Lindsay, Z. H. Aitken, M. T. Pettes, X. Li, Z. Yao, R. Huang, D. Broido, N. Mingo, R. S. Ruoff, and L. Shi, Science **328**, 213 (2010).

[5] C. Lee, X. Wei, J. W. Kysar, and J. Hone, Science **321**, 385 (2008).

[6] A. Bostwick, F. Speck, T. Seyller, K. Horn, M. Polini, R. Asgari, A. H. MacDonald, and E. Rotenberg, Science **328**, 999 (2010).

[7] J. Martin, N. Akerman, G. Ulbricht, T. Lohmann, J. H. Smet, K. von Klitzing, and A. Yacoby, Nature Phys. **4**, 144 (2008).

[8] S. Y. Zhou, G.-H. Gweon, A. V. Fedorov, P. N. First, W. A. de Heer, D.-H. Lee, F. Guinea, A. H. Castro Neto, and A. Lanzara, Nature Mater. **6**, 770 (2007).

[9] M. L. Teague, A. P. Lai, J. Velasco, C. R. Hughes, A. D. Beyer, M. W. Bockrath, C. N. Lau, and N.-C. Yeh, Nano Lett. **9**, 2542 (2009).

[10] F. Guinea, M. I. Katsnelson, and A. K. Geim, Nature Phys. **6**, 30 (2009).

[11] N. Levy, S. A. Burke, K. L. Meaker, M. Panlasigui, A. Zettl, F. Guinea, A. H. Castro Neto, and M. F. Crommie, Science **329**, 544 (2010).

[12] W. Bao, F. Miao, Z. Chen, H. Zhang, W. Jang, C. Dames, and C. N. Lau, Nature Nanotechnol. **4**, 562 (2009).

[13] S. Adam, E. H. Hwang, V. M. Galitski, and S. Das Sarma, Proc. Natl. Acad. Sci. USA **104**, 18392 (2007).

[14] H. Suzuura and T. Ando, Phys. Rev. B **65**, 235412 (2002).

[15] J. M. Poumirol, W. Escoffier, A. Kumar, M. Goiran, B. Raquet, and J. M. Broto, New J. Phys. **12**, 083006 (2010).

[16] Y. Zhang, V. W. Brar, C. Girit, A. Zettl, and M. F. Crommie, Nature Phys. **5**, 722 (2009).

[17] M. Gibertini, A. Tomadin, M. Polini, A. Fasolino, and K. I. Katsnelson, Phys. Rev. B **81**, 125437 (2010).

[18] E. Kim, and A. H. Castro Neto, Europhys. Lett. **84**, 57007 (2008).

[19] A. Fasolino, J. H. Los, and M. I. Katsnelson, Nature Mater. **6**, 858 (2007).

[20] N. Abedpour, R. Asgari, and M. R. Tabar, Phys. Rev. Lett. **104**, 196804 (2010); N. Abedpour, M. Neek-Amal, Reza Asgari, F. Shahbazi, N. Nafari, and M. R. Tabar, Phys. Rev. B **76**, 195407 (2007).

[21] F. de Juan, A. Cortijo, and M. A. H. Vozmediano, Phys. Rev. B **76**, 165409 (2007).

[22] W. Kohn and L. J. Sham, Phys. Rev. **140**, A1133 (1965).

[23] E. Anglada, J. Junquera, and J. M. Soler, Phys. Rev. E **68**, 055701(R) (2003).

[24] D. Marx, and J. Hutter, *Ab Initio Molecular Dynamics Basic Theory and Advanced Methods* (Cambridge University Press, Cambridge, 2009).

[25] S. Nosé, J. Chem. Phys. **81**, 511 (1984); W. G. Hoover, Phys. Rev. A **31**, 1695 (1985).

[26] M. Lazzeri, C. Attaccalite, L. Wirtz, and F. Mauri, Phys. Rev. B **78**, 081406(R) (2008).

[27] J. M. Soler, E. Artacho, J. D. Gale, A. García, J. Junquera, P. Ordejón, and D. Sánchez-Portal, J. Phys.: Condens. Matter **14**, 2745 (2002).

[28] N. Troullier and J. L. Martins, Phys. Rev. B **43**, 1993 (1991).

[29] H. J. Monkhorst and J. D. Pack, Phys. Rev. B **13**, 5188 (1976).

[30] J. P. Perdew, K. Burke, and M. Ernzerhof, Phys. Rev. Lett. **77**, 3865 (1996).

[31] We had to choose the smaller sample for the accurate electronic structure calculations because of limited computational power.

[32] M. P. Wand and M. C. Jones, *Kernel smoothing* (Chapman & Hall, London, 1995); F. Ghasemi, J. Peinke, M. Sahimi, and M. Reza Rahimi Tabar, Eur. Phys. J. B **47**, 411 (2005).

[33] W. J. Zakrzewski, J. Nonlin. Math. Phys. **12**, 530538 (2005).

[34] In order to find the wavelength of the ripples, we considered $\sum_i \langle |Z(i+a) - Z(i)|^2 \rangle$ as a function of a, where i is the index of the atoms in the sample [G. R. Jafari, S. M. Fazeli, F. Ghasemi, S. M. Vaez Allaei, M. R. Tabar, A. Iraji Zad, and G. Kavei, Phys. Rev. Lett. **91**, 226101 (2003)]. The first minimum gives the wavelength. This minimum could be observed in samples consisting of more than 392 atoms and occurs approximately for the same index a along the side of the supercell. Projecting the index for the first minimum on the longer diagonal of the diamond-shaped unit cell and performing the same calculation on other directions, we obtained the value of $\simeq$55 Åfor the ripple wavelength.